Supporting Materials for

Imaging Grain Structure in Halide Perovskites: Local Crystal Misorientation Influences Non-Radiative Recombination

Sarthak Jariwala[1,2], Hongyu Sun[3], Gede W. P. Adhyaksa[3], Andries Lof[3], Loreta A. Muscarella[3], Bruno Ehrler[3], Erik C. Garnett[3], David S. Ginger[1]*

[1] Department of Chemistry, University of Washington, Seattle, WA 98195

[2]Department of Materials Science and Engineering, University of Washington, Seattle, WA 98195, USA

[3]Center for Nanophotonics, AMOLF, 1098 XG, Amsterdam, The Netherlands

*Corresponding Author: dginger@uw.edu

Note S1.

Electron Back-Scatter Diffraction (EBSD)

The individual Kikuchi patterns acquired from EBSD were indexed to a tetragonal MAPI structure with I4/mcm space group symmetry.[1,2] The lattice parameters used were a = b = 8.84 Å and c = 12.63 Å. The overall absolute error in orientation determination was calculated using average fit to be 1.8° (typically, the accuracy of absolute orientation determination is ~2°).[3] Average fit describes the average angular difference between the detected Kikuchi bands in the diffraction pattern and the corresponding bands reconstructed from the orientation solution.[4] The average fit value is heavily dependent on the pattern quality and the Kikuchi band detection parameters.[5] However, when detecting sub-grain microstructures, the accuracy of relative orientations between adjacent data points is more important.[3] The relative angular resolution was measured by scanning across a Si (100) single crystal. The orientation noise or the angular resolution was found to be <1° for 90% of the points. The beam conditions were 6 kV accelerating voltage, 800 pA beam current and 0.2 s exposure.

Post indexing, the EBSD data was analyzed and plotted using MTEX, an open-source MATLAB toolbox for texture/orientation analysis.[6,7]

Kikuchi Diffraction Patterns Analysis

We process the data using a home script to remove background, optimize brightness and contrast, and balance the signal in 4 quadrants of the detector. The boundaries between the 4 quadrants of the detector are also removed to prevent it from being recognized as a diffraction line. Using OIM Analysis Software from EDAX, the patterns are corrected to reduce the noise levels using Neighbor Pattern Averaging & Reindexing (NPAR) method prior to indexing.

The Kikuchi patterns are also calibrated with an Aluminum metal sheet at the same working distance as the perovskite sample. Next, we optimize Hough transform by adjusting convolution mask, maximum band count, Rho fraction. After indexing, we correct pseudosymmetry and correct non-indexed points with grain dilation function. Lastly, we further improve image with Neighbor Orientation Correlation.

Grain Detection using MTEX

During grain identification from raw inverse pole figure (IPF), pixelated regions are first identified and removed. These are the points that the grain detection algorithm identifies as one pixel grain, and since that is likely a random measurement point/indexing error, they are removed from the map.

Once these pixels are removed from the EBSD map, a grain threshold angle is selected, and grain identification is performed using MTEX texture analysis package. According to the MTEX algorithm,[8] missing data due to measurement errors (here the removed pixels) do not interfere in the grain detection process.[8] Briefly, in the MTEX algorithm, there is no systemic bias in the assignment of these missing orientations and, they do not cause the grain to be split into different grains. The missing orientation data are equally assigned to neighboring points.

Importantly, since the pixels are removed, they do not contribute to or interfere in any further analysis of grains, grain boundaries, grain orientation spread, etc.

Post grain detection, we plot the mean grain orientation along with the grain boundaries. The above process is depicted in Figure S8.

Note S2.

Aligning Confocal Photoluminescence (PL) Images and EBSD maps

First, a region of interest (ROI) was formed by using Atomic Force Microscope (AFM) tip in contact mode to precisely scratch through the perovskite film. The ROI size was defined by AFM controls in x and y direction. After ROI was formed, confocal PL was performed on the ROI and silver paint was then deposited on the sides of the film for EBSD. Then, EBSD was performed on the same ROI to generate a local crystal orientation map.

Using an image registration program written in python using packages such as scikit-image[9] and OpenCV, the confocal PL maps and EBSD maps were aligned keeping ROI fiducial markers as known reference points across the two maps. Image registration between PL and EBSD was achieved by using fiducial markers followed by affine transformation (to account for resolution differences, beam angle etc). Post alignment, the PL and EBSD were overlaid to map the grain orientation spread of the grains to their corresponding local PL. Since the analysis requires correlation with PL, grains that were not optically resolved (smaller than the resolution limit of the microscope) were not considered for the analysis. Furthermore, grains right beside the scratch were also not considered for the analysis due to possible mechanical damage from scratching. The data were binned in intervals of GOS to create a plot of average PL intensity as a function of GOS.

Note S3.

Hypothesis testing and p-value

In inferential statistics, hypothesis testing is used to deduce relationships between the underlying distributions. The most common test is the null hypothesis (H_0) versus the alternate hypothesis (H_a) test. H_0 assumes that there is no relationship between underlying distributions, say X and Y. H_a assumes that there is some relationship between the distributions.[10]

The p-value is the probability of the occurrence of a given event within a statistical hypothesis test. In other words, the p-value indicates the probability of uncorrelated distributions (X and Y) producing the same correlation as determined from the correlated distributions, X and Y.

The interpretation of p-value is as follows: a small p-value (generally, $p<0.05$ or 5%) indicates that it is *unlikely* that any association between the distributions (X & Y) exists due to *random chance*. Therefore, if we see a small p-value ($p<0.05$), we can infer that there is a relationship between the distributions, and we can reject the null hypothesis. In other words, a small p-value ($p<0.05$) indicates that there is statistically significant relationship between X and Y.[10] On

the contrary, if the p-value is greater than 0.05, we can infer that the relationship between the distributions is not statistically significant and we cannot reject the null hypothesis.[10] We note that a p-value larger than the threshold (0.05) does not imply there is simply *no relationship* between the distributions. But, instead, the hypothesis under investigation does not adequately explain the observations.

We also note that although the choice of p-value threshold of 0.05 is most commonly used, it is an arbitrary convention.

The correlations and p-values were calculated using scipy (scipy.stats) library in python.[11]

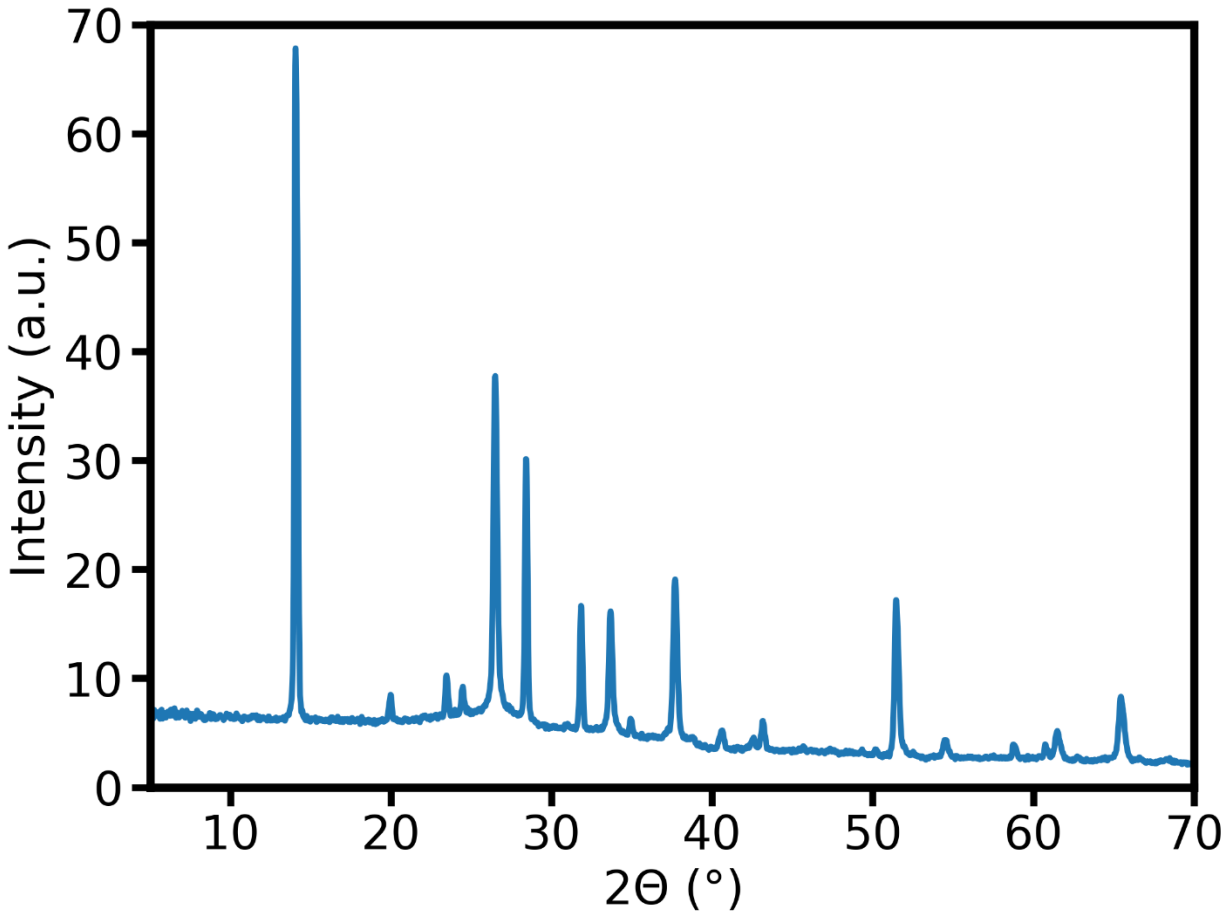

Figure S1. XRD plot of a representative $CH_3NH_3PbI_3$ thin film on FTO substrate demonstrating the crystallinity of the film.

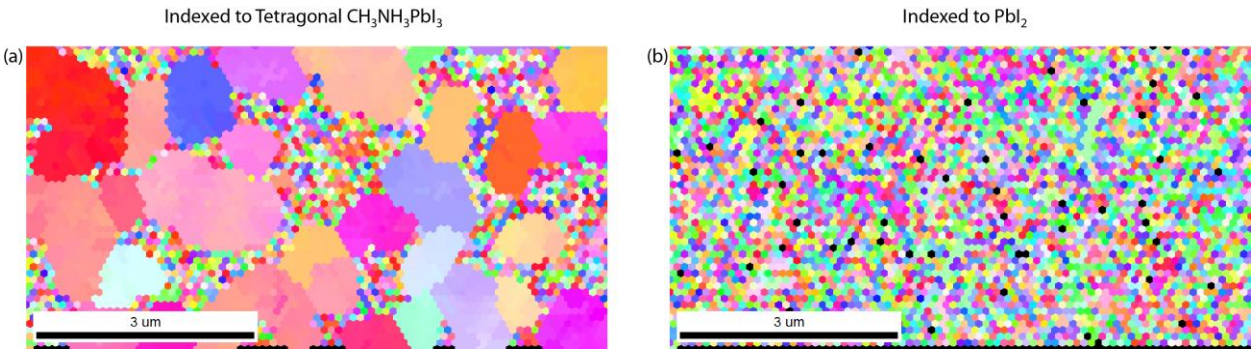

Figure S2. Inverse Pole Figure of $CH_3NH_3PbI_3$ thin films with individual back scatter diffraction patterns indexed to (a) tetragonal $CH_3NH_3PbI_3$ structure and (b) hexagonal PbI_2 for the same scan region.

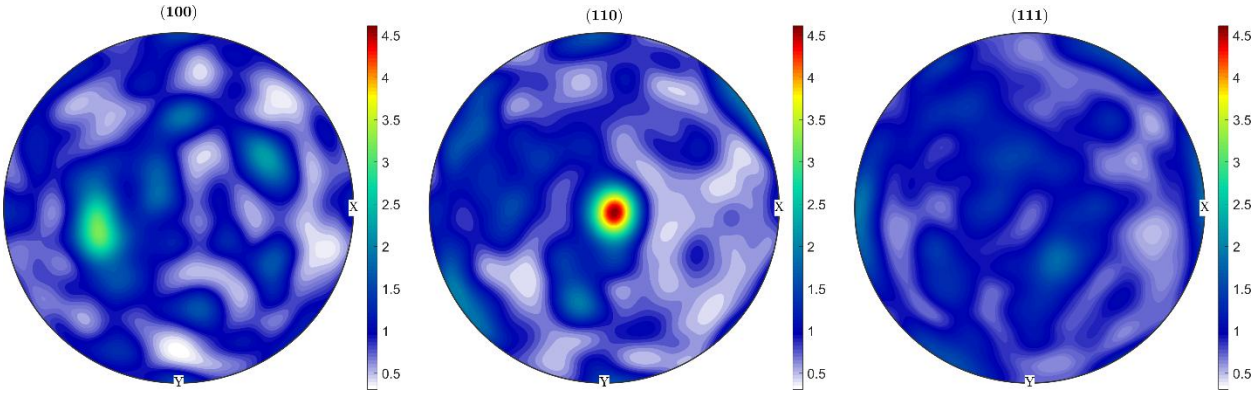

Figure S3. Pole Density Figure. Projection of crystal orientations into the sample coordinate system. The color bars represent multiples of random distribution of orientations, meaning pole figure of a random standard sample would be '1x' at all points. Pole figure regions with intensities higher than '1x' demonstrate lattice planes that are preferentially aligned in those directions compared to a sample with random texture.

a)

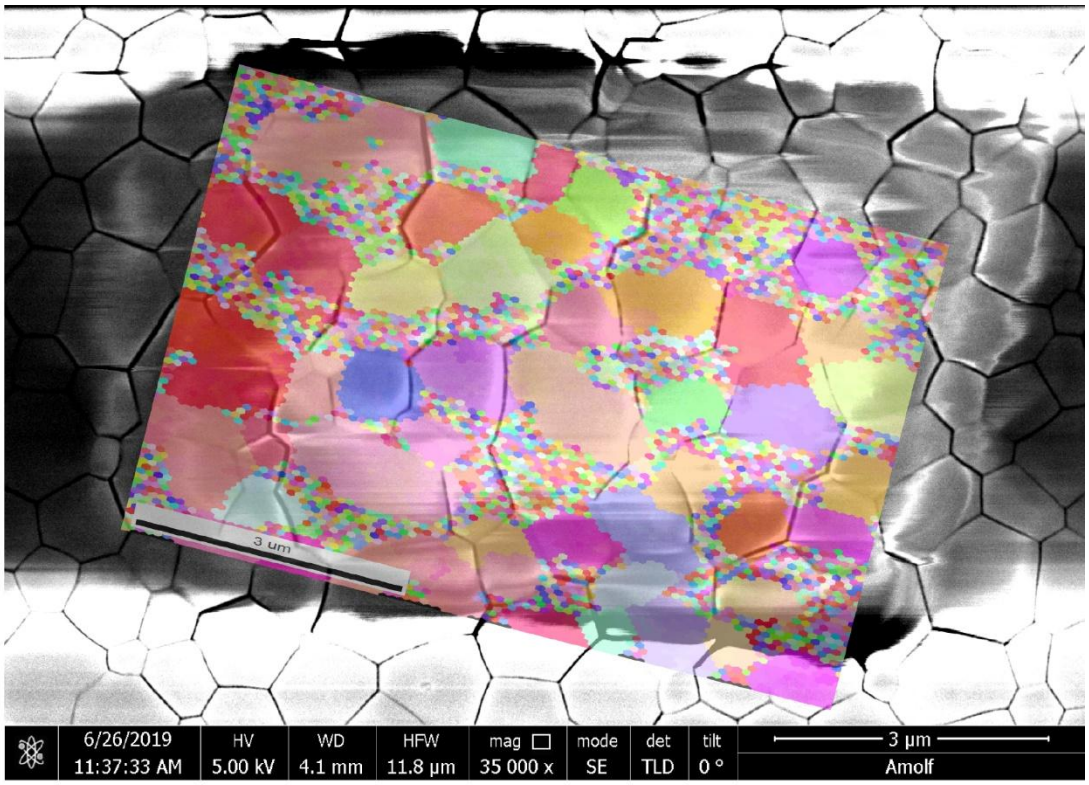

b)

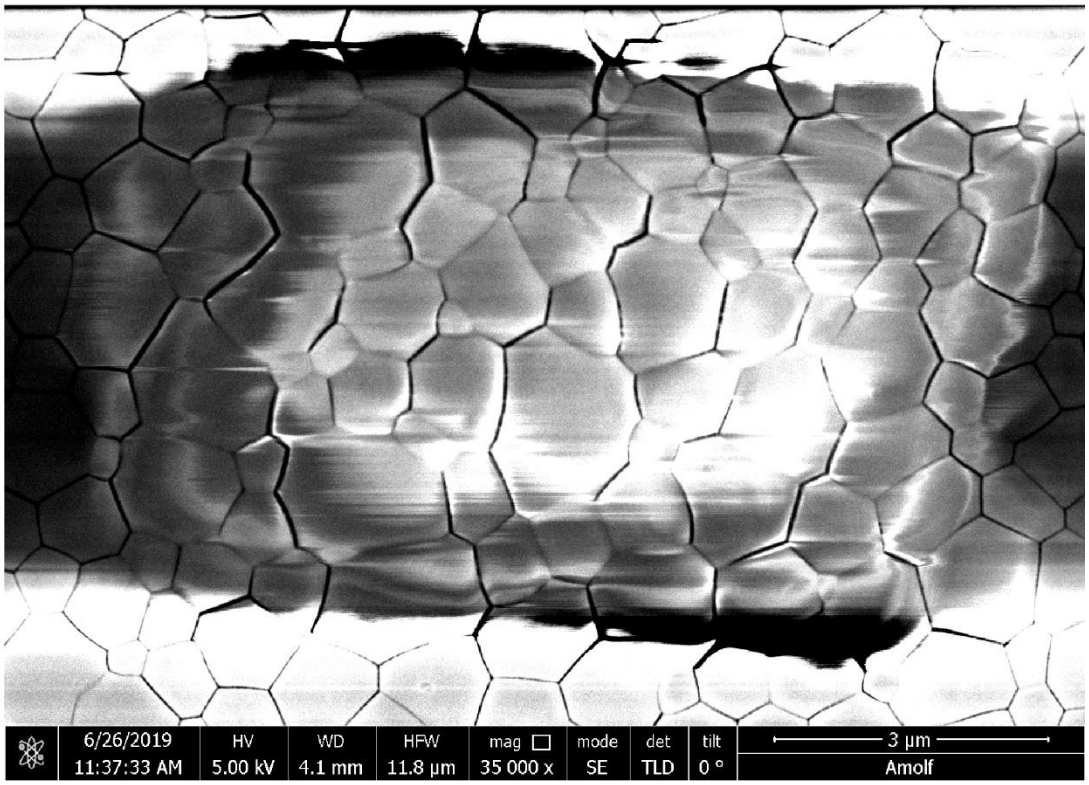

Figure S4. Conventional SEM image at 0 degrees tilt and EBSD of the corresponding region. (a) Inverse Pole Figure (IPF) overlaid on top of the high-resolution SEM image. (b) High-resolution SEM image acquired after EBSD measurement. The white regions are due to charging effects.

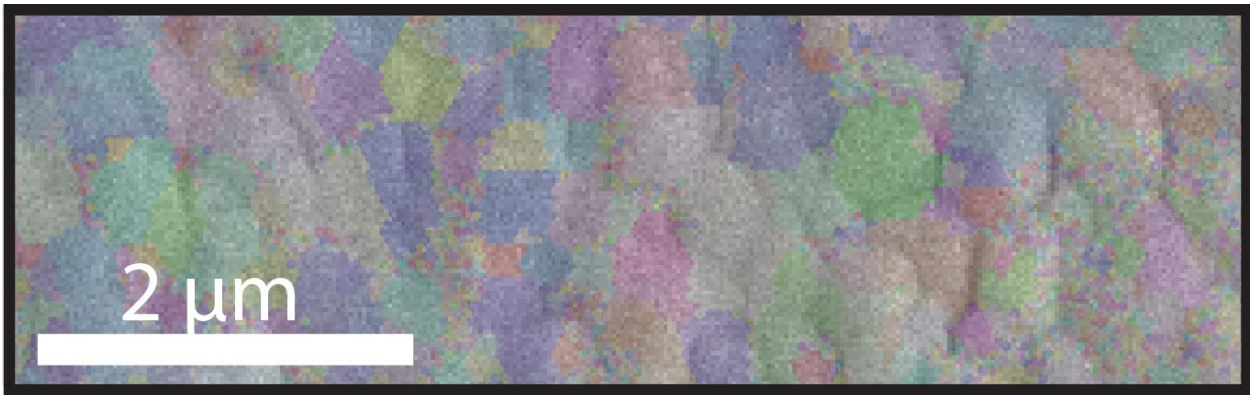

Figure S5. Overlay of scanning electron microscope image and inverse pole figure (IPF) shown in Figure 1b and 1c in the main text.

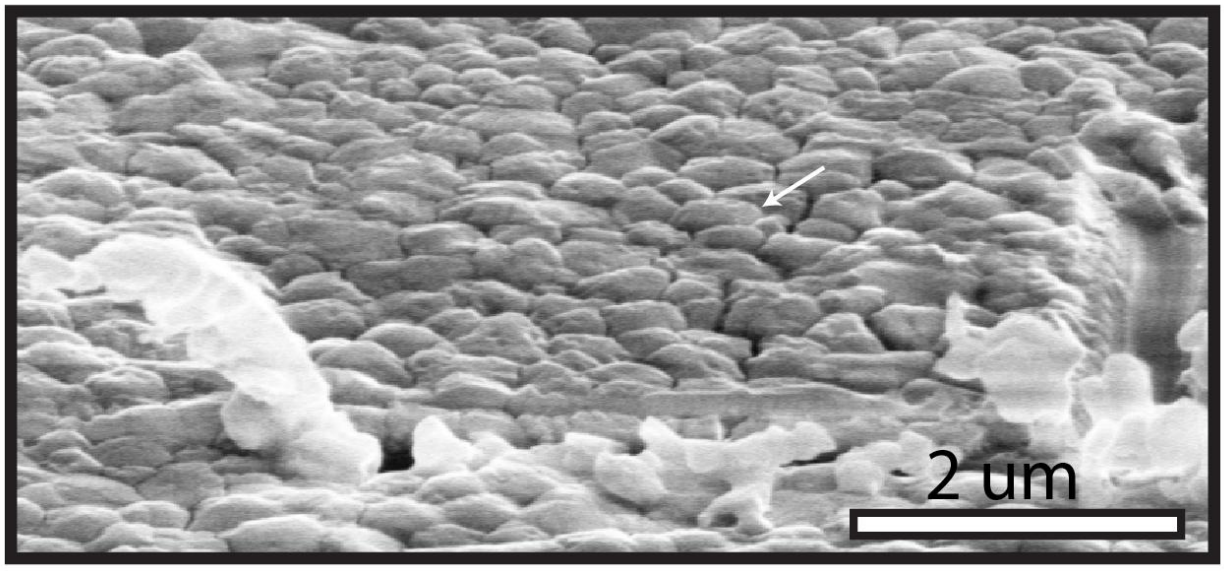

Figure S6. Higher resolution SEM image (at 40° tilt) of the region in Figure 1b in the main text with scratch markers defining the ROI. The arrow shows the same region along the arrow in Figure 1b.

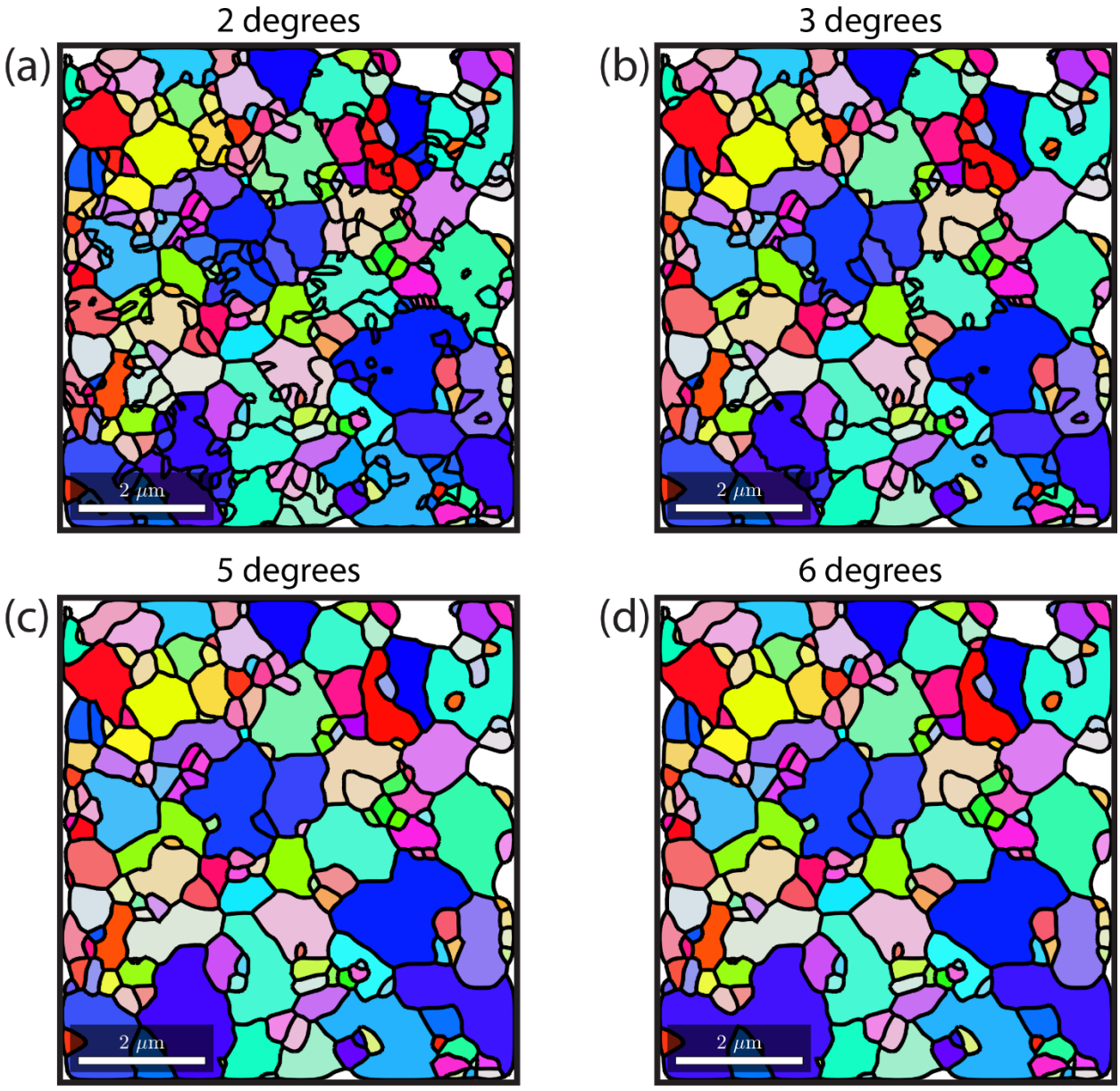

Figure S7. Grain identification from IPF using different misorientation thresholds of (a) 2 degrees, (b) 3 degrees, (c) 5 degrees and (d) 6 degrees. Grains are plotted with their mean orientation. Refer Figure 2 in the main text for 4 degrees grain threshold and for color key.

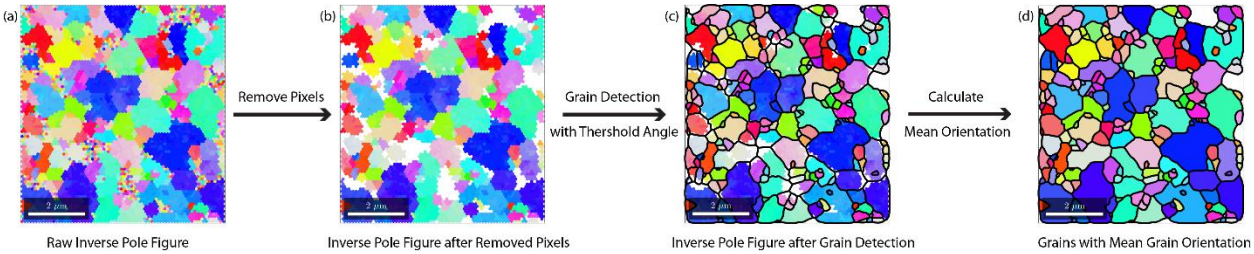

Figure S8. Grain identification process from raw inverse pole figure (IPF) to grains with mean orientation. (a) Raw IPF. (b) IPF after pixelated regions corresponding to one pixel grain are removed from the map. (c) Grain detection performed on resulting IPF from (b) with a threshold angle. The IPF is plotted with corresponding grains and grain boundaries that were identified. (d) Grain mean orientation is calculated and plotted with the corresponding grain boundaries.

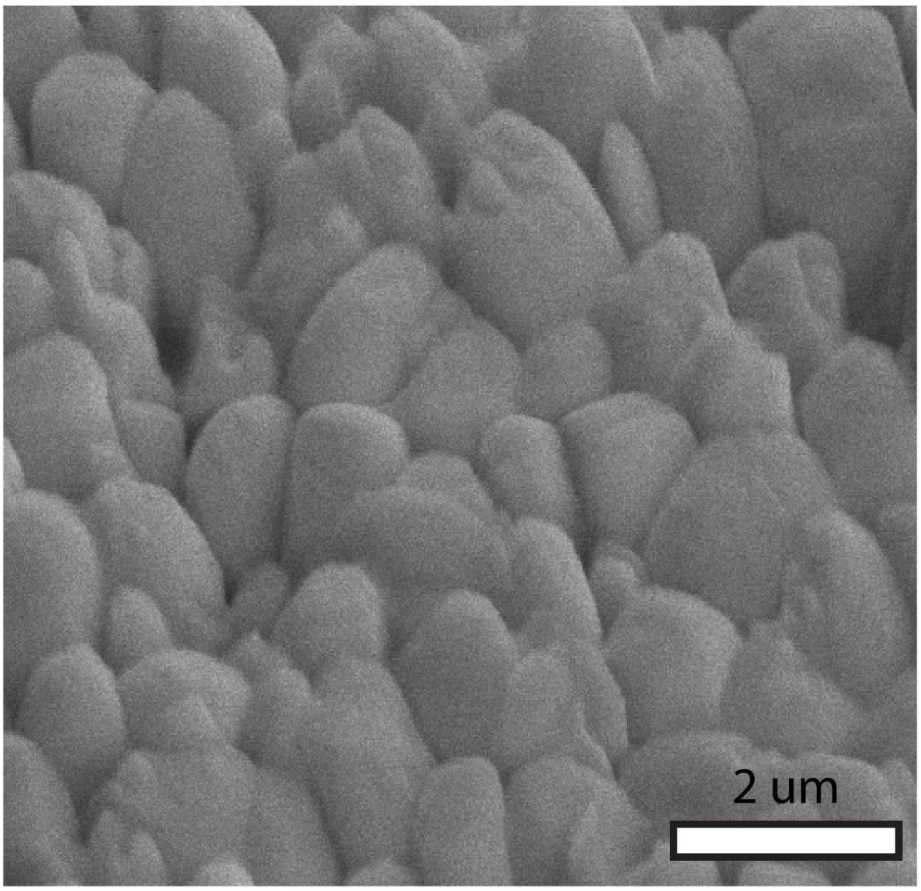

Figure S9. SEM image at 40° tilt of $CH_3NH_3PbI_3$ thin film for the region in Figure 2 in the main text.

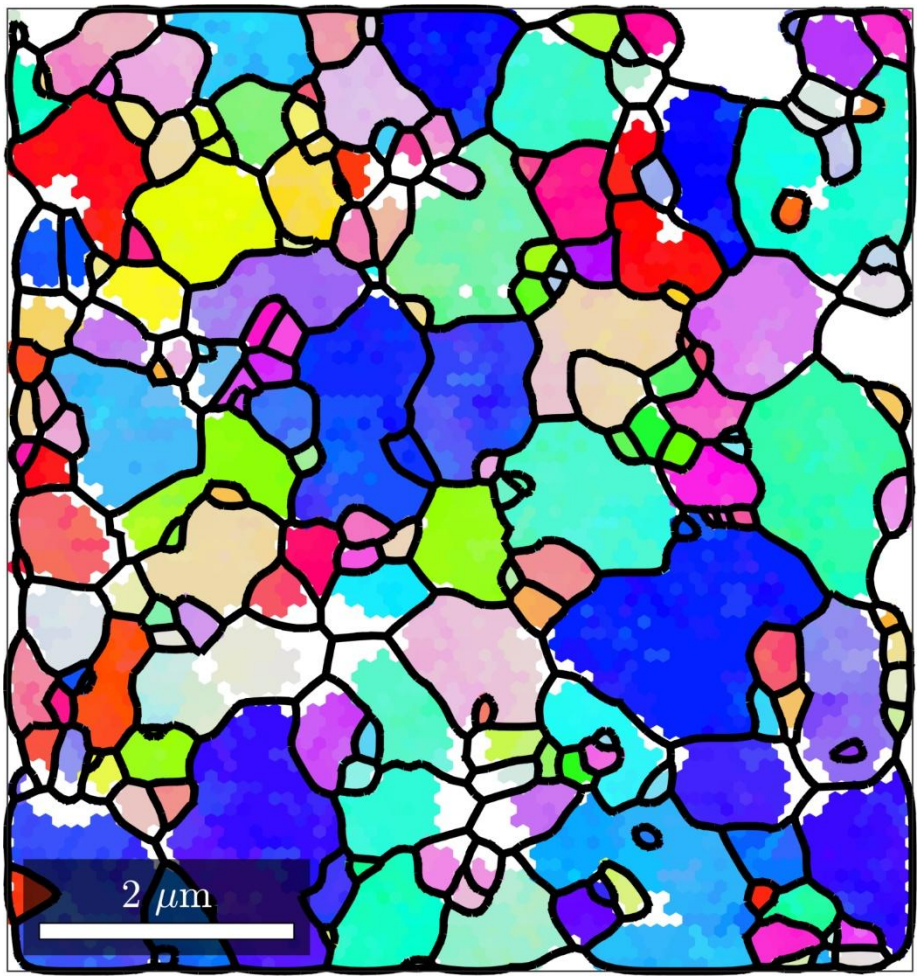

Figure S10. Inverse Pole Figure (IPF) with grain boundaries after grain detection showing grain-to-grain orientation heterogeneity within the film. See Figure 2a and 2b in main text for IPF and plot of grains with mean orientation.

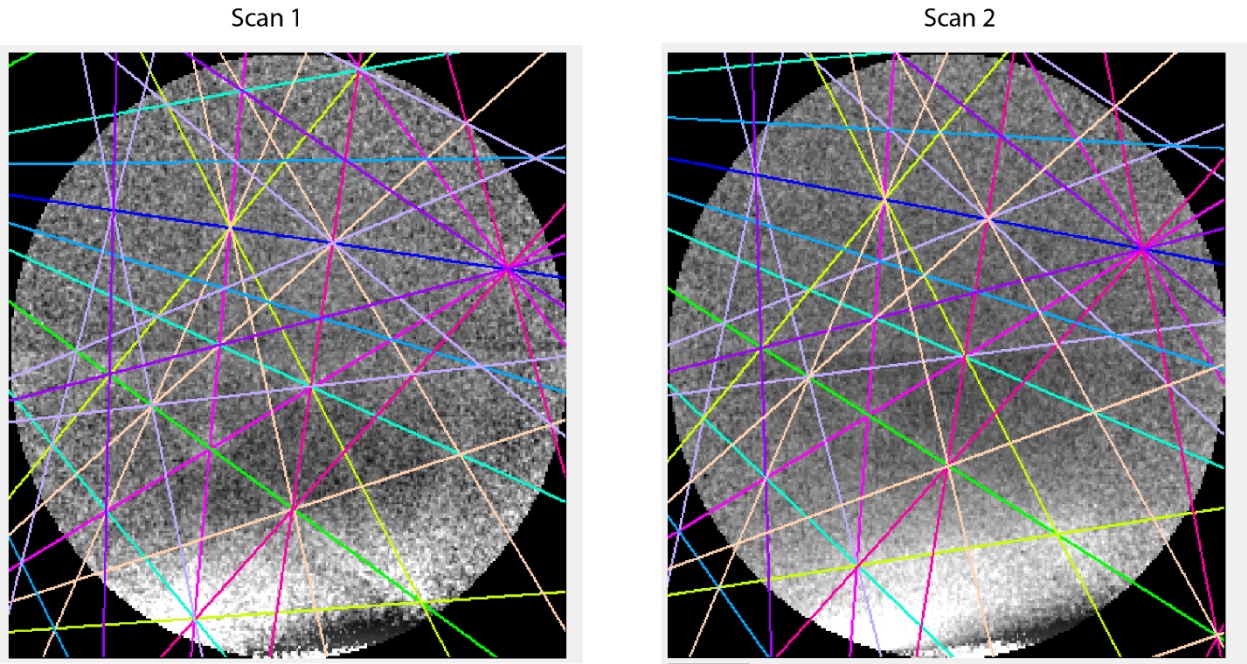

Figure S11. Electron back scatter diffraction patterns of the same region from two consecutive scans showing that the pattern is present and indexed to the same crystallographic orientation of tetragonal $CH_3NH_3PbI_3$ after consecutive scans and, thus, demonstrating the minimal influence of electron beam induced damage on the overall results interpreted from the diffraction patterns.

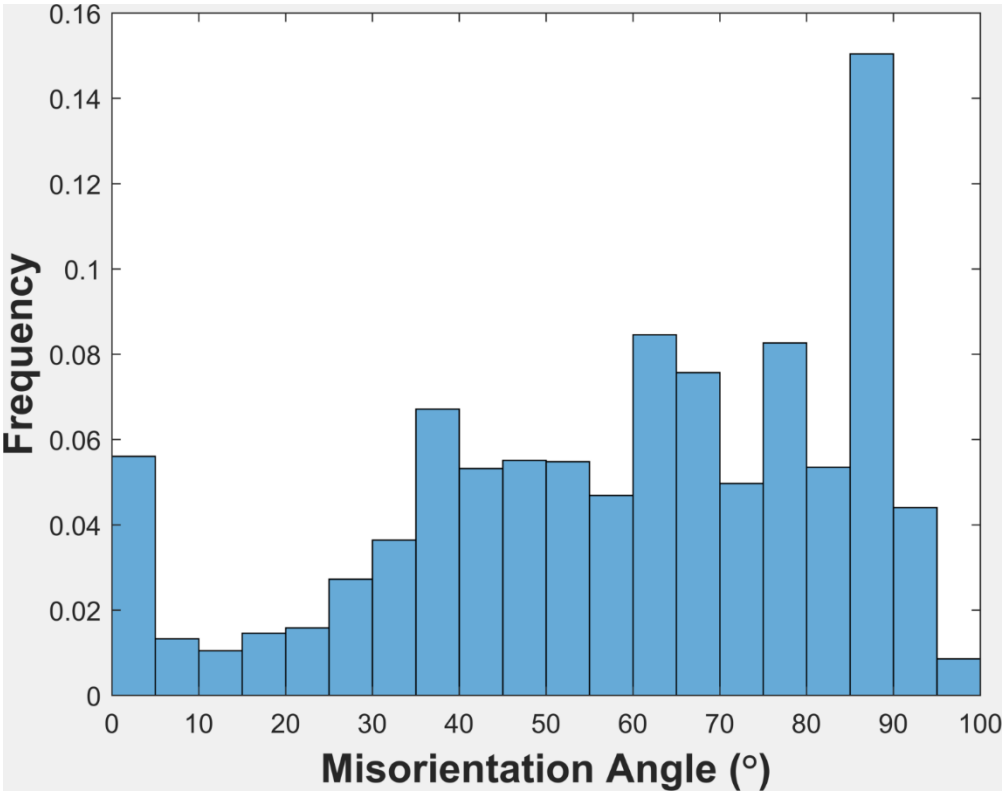

Figure S12. Misorientation angle histogram showing the distribution of grain boundary misorientation angle in a representative $CH_3NH_3PbI_3$ thin film.

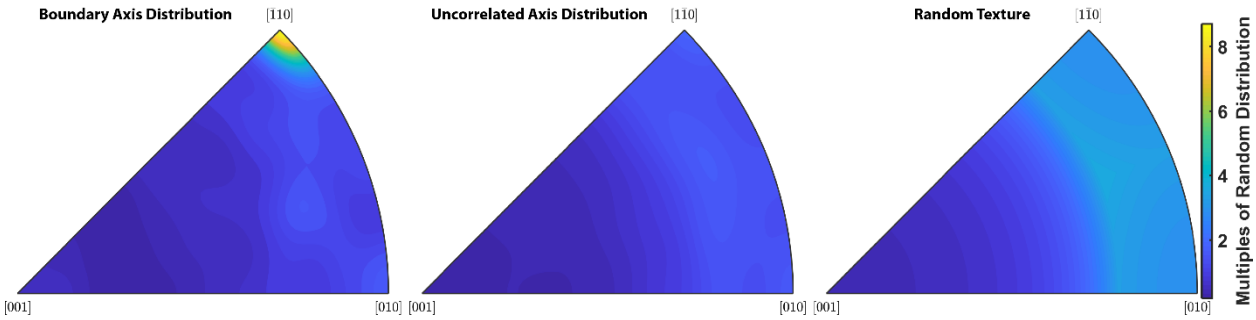

Figure S13. Grain boundary misorientation axis distribution showing preferred orientation along [110] direction. Uncorrelated axis distribution is calculated using the uncorrelated misorientation (from points far from each other) and the underlying orientation distribution function. Misorientation axis distribution for random texture was calculated using random orientation distribution and crystal symmetry in the film.

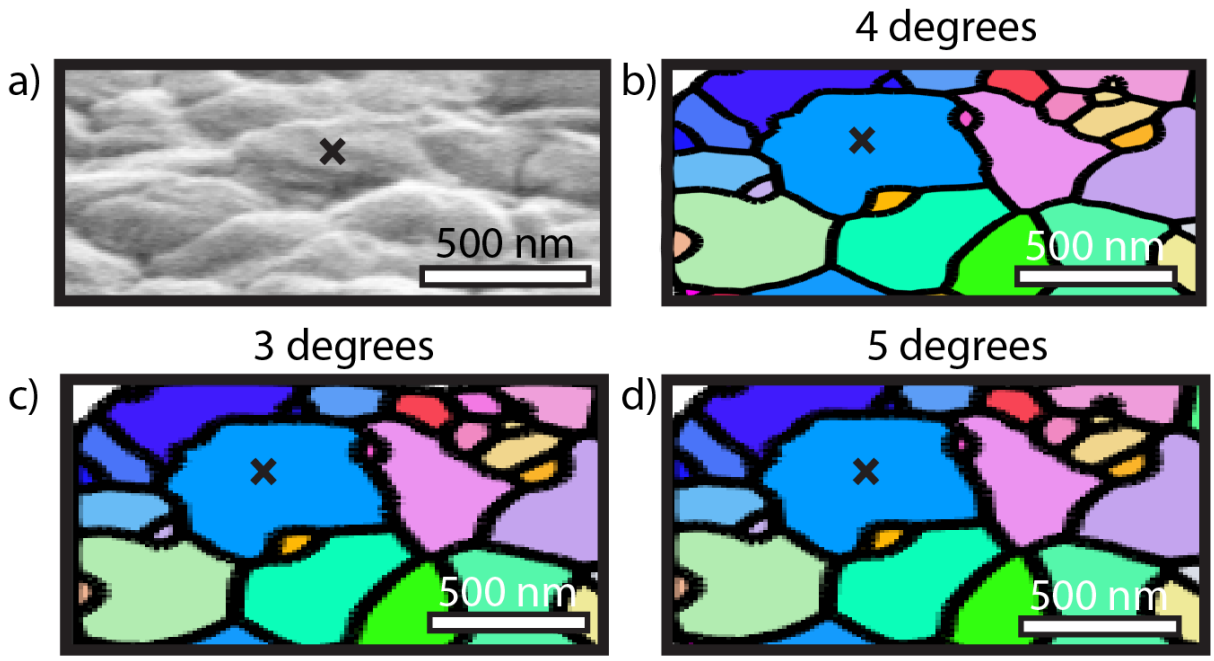

Figure S14. (a) SEM image at 40 degrees tilt and corresponding grains identified at different thresholds; (b) 4 °, (c) 3 ° and (d) 5 °; and plotted with their mean grain orientation. The grain marked with "X" represents the grain in Figure 3a in the main text.

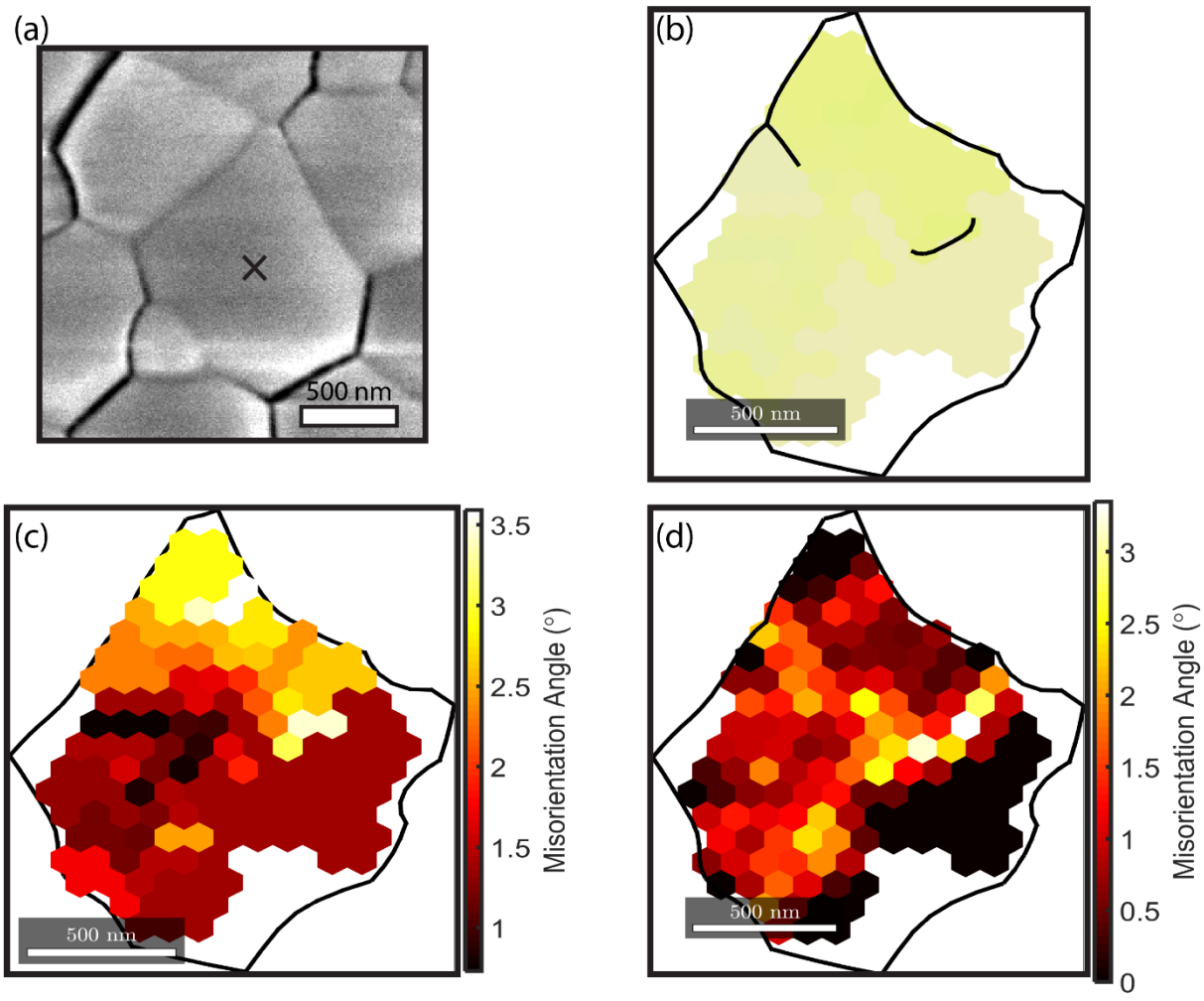

Figure S15. (a) High-resolution SEM image of a grain along with (b) Inverse Pole Figure (IPF) with sub-grain boundaries. (c) Kernel average misorientation (KAM) and (d) misorientation with respect to mean grain orientation of the same grain in (a) and (b). The grains were identified using a 4° threshold. The grains in (b), (c) and (d) correspond to the grain marked with "X" in the (a).

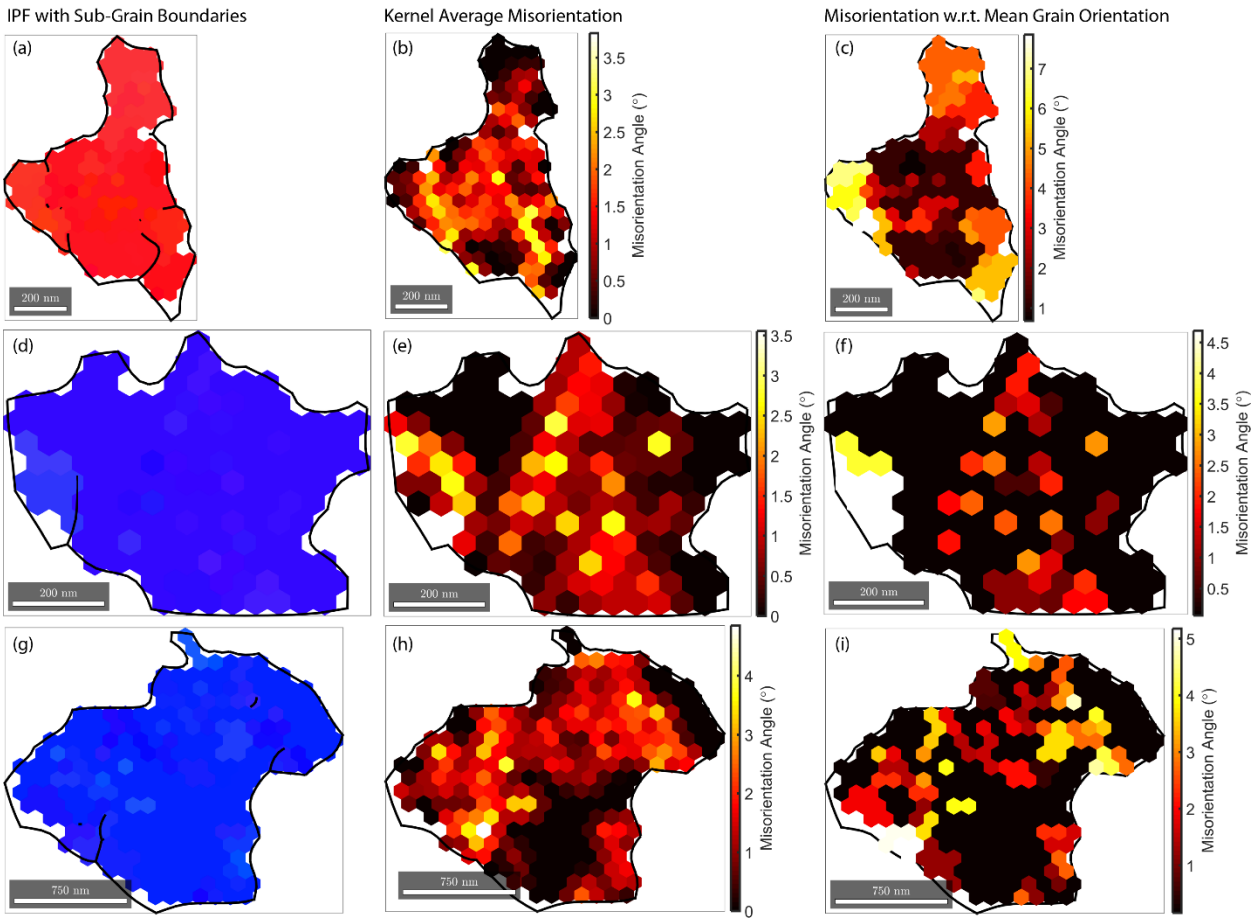

Figure S16. Inverse Pole Figure (IPF) with sub-grain boundaries (a, d, g), kernel average misorientation (b, e, h) and misorientation with respect to mean grain orientation (c, f, i) for three different grains from different EBSD scans.

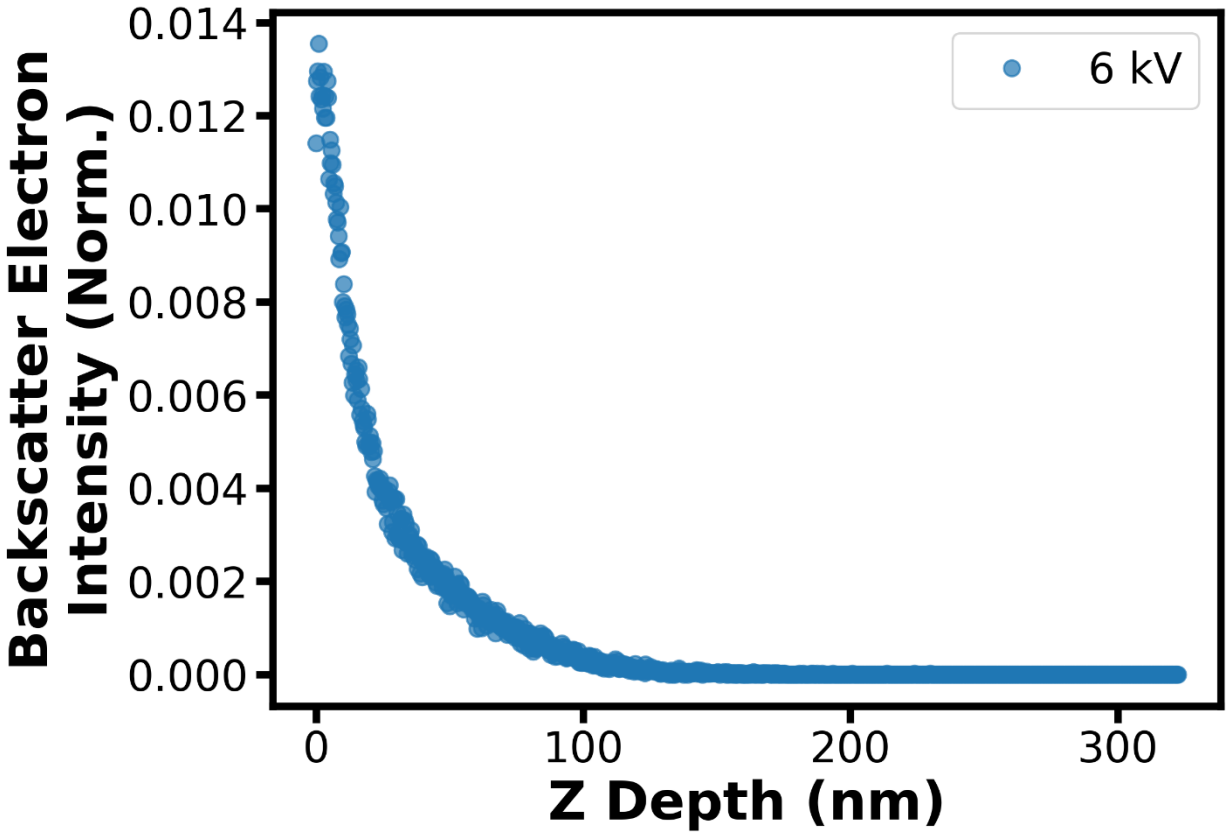

Figure S17. Monte-Carlo simulation (using CASINO[12]) of electron interaction with $CH_3NH_3PbI_3$ showing backscatter electron intensity as a function of z-depth in the film at 6kV accelerating voltage. The simulation was performed in traditional EBSD geometry (70° electron incidence with respect to the surface normal). This shows that the traditional EBSD geometry is more surface sensitive with a higher probability of backscattered electrons escaping from the perovskite surface.

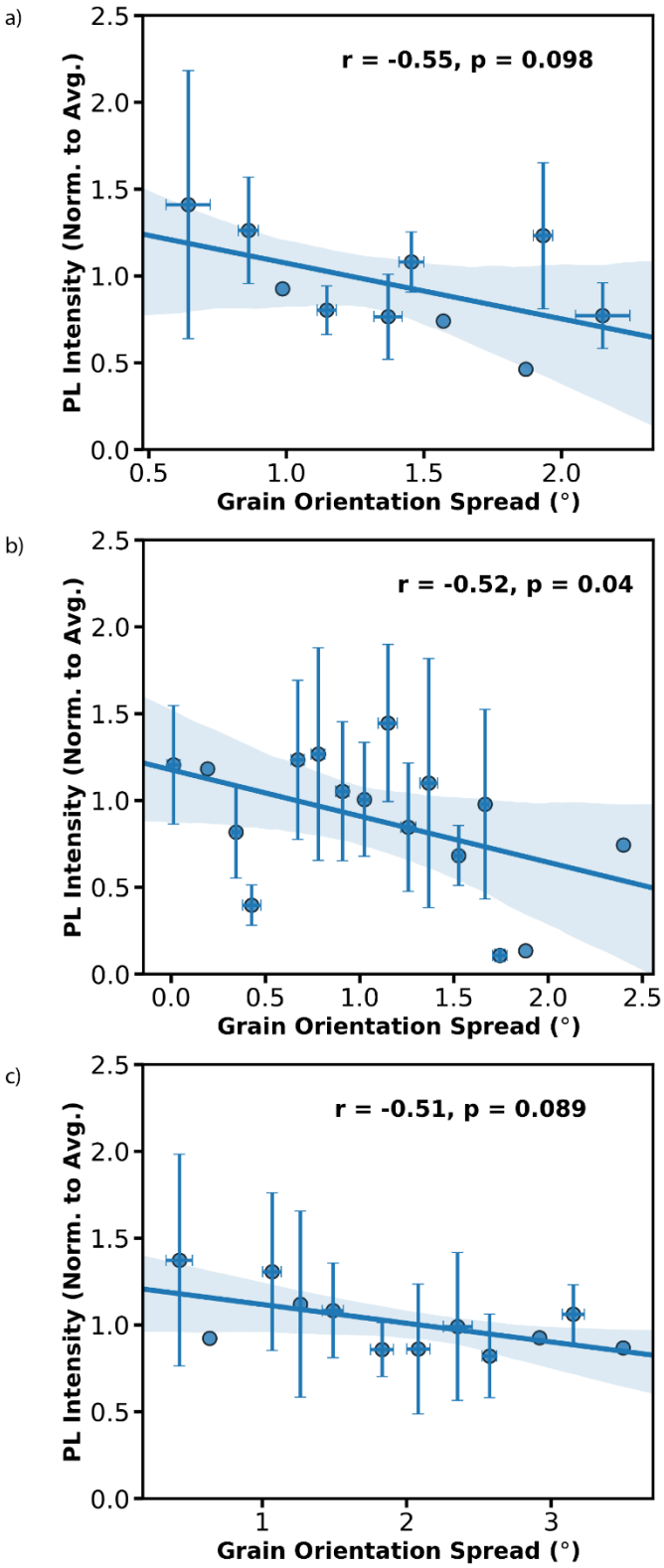

Figure S18. Correlation plot of PL intensity as a function of grain orientation spread (GOS) showing negative correlation for three different sample sets individually comprising of (a) 25 grains, (b) 80 grains and (c) 38 grains. The plots show anti-correlation with the line

representing a linear regression fit to the data and shaded region representing 95% confidence interval. Error bars represent the standard deviation of the average PL intensity in a specific GOS interval.

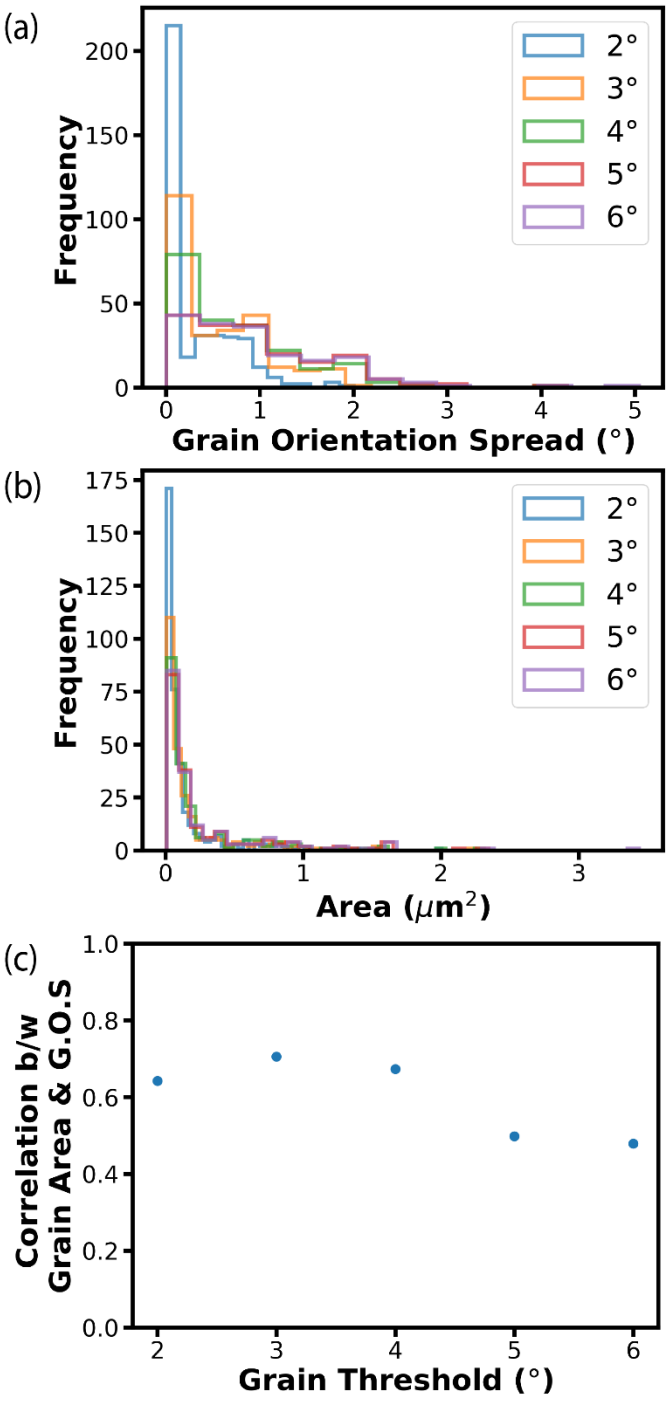

Figure S19. Histograms of (a) grain orientation spread (GOS) and (b) grain area for different grain threshold values. (c) Correlation between grain area and GOS at different threshold values showing strong positive correlation at all different grain threshold values.

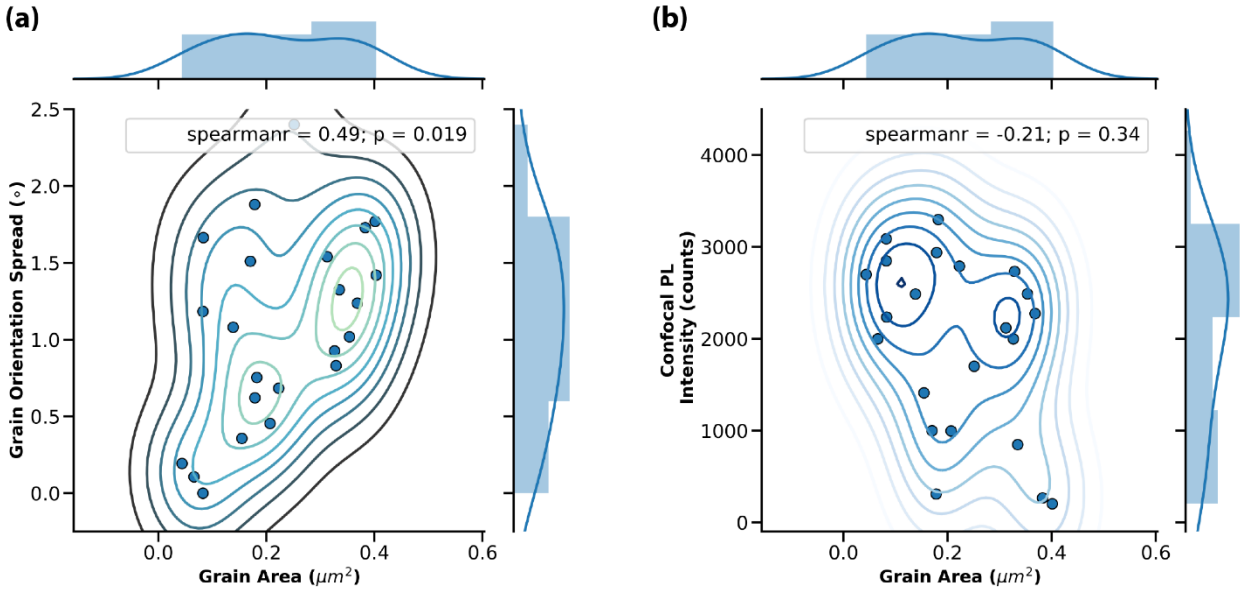

Figure S20. (a) Grain orientation spread within grains as a function of grain area showing positive correlation with high statistical significance (p = 0.019; p<0.05). (b) PL intensity measured at fluence corresponding to local trap density (see main text for more details) as a function of grain area showing very weak negative correlation with very low statistical significance (p = 0.34; p>0.05). The contours in (a) and (b) represent the kernel density estimate.

References:

[1] Poglitsch A, Weber D. Dynamic disorder in methylammoniumtrihalogenoplumbates (II) observed by millimeter-wave spectroscopy. J. Chem. Phys. 1987;*87*:6373–8. doi:10.1063/1.453467.

[2] Baikie T, Fang Y, Kadro JM, Schreyer M, Wei F, Mhaisalkar SG, et al. Synthesis and crystal chemistry of the hybrid perovskite (CH3NH3)PbI3 for solid-state sensitised solar cell applications. J. Mater. Chem. A 2013;*1*:5628. doi:10.1039/c3ta10518k.

[3] Humphreys FJ, Huang Y, Brough I, Harris C. Electron backscatter diffraction of grain and subgrain structures - resolution considerations. J. Microsc. 1999;*195*:212–6.

[4] Krieger Lassen NC. Source point calibration from an arbitrary electron backscattering pattern. J. Microsc. 1999;*195*:204–11. doi:10.1046/j.1365-2818.1999.00581.x.

[5] Nowell MM, Wright SI. Orientation effects on indexing of electron backscatter diffraction patterns. Ultramicroscopy, vol. 103, 2005, p. 41–58. doi:10.1016/j.ultramic.2004.11.012.

[6] Bachmann F, Hielscher R, Schaeben H. Texture Analysis with MTEX – Free and Open Source Software Toolbox. Solid State Phenom. 2010;*160*:63–8. doi:10.4028/www.scientific.net/SSP.160.63.

[7] Nolze G, Hielscher R. Orientations - Perfectly colored. J. Appl. Crystallogr. 2016;*49*:1786–802. doi:10.1107/S1600576716012942.

[8] Bachmann F, Hielscher R, Schaeben H. Grain detection from 2d and 3d EBSD data-Specification of the MTEX algorithm. Ultramicroscopy 2011;*111*:1720–33. doi:10.1016/j.ultramic.2011.08.002.

[9] van der Walt S, Schönberger JL, Nunez-Iglesias J, Boulogne F, Warner JD, Yager N, et al. scikit-image: image processing in Python. PeerJ 2014;*2*:e453. doi:10.7717/peerj.453.

[10] James G, Witten D, Hastie T, Tibshirani R. An Introduction to Statistical Learning with Applications in R. n.d.Springer; . doi:10.1007/978-1-4614-7138-7.

[11] Jones, E., Oliphant, E., Peterson P et al. SciPy: Open Source Scientific Tools for Python 2001.

[12] Demers H, Poirier-Demers N, Couture AR, Joly D, Guilmain M, de Jonge N, et al. Three-dimensional electron microscopy simulation with the CASINO Monte Carlo software. Scanning 2011;*33*:135–46. doi:10.1002/sca.20262.